Available online at www.sciencedirect.com
ScienceDirect
Journal of Pharmaceutical and Biomedical Analysis 46 (2008) 36–44
JOURNAL OF PHARMACEUTICAL AND BIOMEDICAL ANALYSIS
www.elsevier.com/locate/jpba

Density mapping and chemical component calibration development of four-component compacts via terahertz pulsed imaging

Ryanne Palermo [a], Robert P. Cogdill [b], Steven M. Short [a], James K. Drennen III [a,*], Philip F. Taday [c]

[a] *Duquesne University Graduate School of Pharmaceutical Sciences, 410A Mellon Hall, 600 Forbes Ave., Pittsburgh, PA 15282, United States*
[b] *Duquesne University Center for Pharmaceutical Technology, 410A Mellon Hall, 600 Forbes Ave., Pittsburgh, PA 15282, United States*
[c] *TeraView Limited, Platinum Building, St. John's Innovation Park, Cowley Road, Cambridge CB4 OWS, UK*[1]

Received 13 August 2007; received in revised form 15 October 2007; accepted 17 October 2007
Available online 23 October 2007

Abstract

The purpose of this research was to investigate suitable procedures for generating multivariate prediction vectors for quantitative composition and density analysis of intact solid oral dosage forms using terahertz pulsed imaging (TPI) spectroscopy. Both frequency- (absorbance and refractive index) and time-domain data are presented. A set of calibration and prediction samples were created according to a quaternary mixture design with five levels of compaction at each concentration design point. Calibration models were generated by partial least-squares, type II (PLS-2) regression of the TPI spectra against nominal composition and relative density reference measurements. Quantitative frequency-domain composition calibration models were created for all crystalline components ($R^2 > 0.90$), but the calibration models for individual amorphous components ($R^2 < 0.76$) did not perform as well in testing. Combining both amorphous components into a single component variable for regression resulted in lower error statistics and equally good predictions of crystalline components. A non-linear attenuation of time-domain spectra was observed as a function of compaction force, which corresponded to compact density predictions ($R^2 = 0.948$). While refractive index spectra were sensitive to density ($R^2 = 0.937$), the absorbance spectra were not. Surface density maps were prepared based on refractive index calibrations.

Keywords: Terahertz; Spectroscopy; Chemical mapping; Partial least squares; Chemometrics; Tablet density

1. Introduction

The technology of generating and detecting ultrashort and coherent electromagnetic pulses in the terahertz (THz) region permits a practical method of chemical imaging with far-infrared radiation. The broadband spectral nature of these pulses permits recording of the dielectric function (absorption coefficient and index of refraction) from the modification of the shape of an electromagnetic pulse transmitted through a sample [1]. The technique also exploits the sub-picosecond pulse length to implement time-gated detection which enables depth-resolved measurements of some optical properties. The instrumental design and implementation used to accomplish these objectives are well described [2,3].

The use of chemometric techniques in combination with terahertz spectroscopic data to generate predicted chemical images of pharmaceuticals is relatively new. Watanabe et al. [4] demonstrated a method for inspection of pelletized chemical mixtures by THz spectroscopic imaging using known spectral data of the pure components. Their routine, based on principle component analysis (PCA) and non-linear regression with a non-negative constraint, was able to identify constituents, map their spatial distributions in powder mixtures, and estimate constituent content. However, the frequency range used for the analysis was very small (1.3–1.8 THz, which corresponds to a window of approximately 16.5 cm^{-1}), and each component had distinct spectral THz signatures, so the complexity of their problem was low. The authors noted that because THz waves are attenuated mainly by absorption, the THz image shows absorbance that is proportional to the concentration and the thickness of the chemical samples. In an earlier paper, they concluded that the image observed at a THz frequency can be expressed as a linear combination of absorbance spectra and spatial patterns [5].

* Corresponding author.
E-mail addresses: drennen@duq.edu, forchtr@duq.edu (J.K. Drennen III).
[1] http://www.teraview.com.

0731-7085/$ – see front matter © 2007 Elsevier B.V. All rights reserved.
doi:10.1016/j.jpba.2007.10.023

Shen et al. [3] combined structural maps of samples obtained by analyzing THz time-domain data with chemical maps obtained from THz spectral (frequency-domain) data to produce three-dimensional chemical maps of pellets using terahertz pulsed imaging (TPI) spectroscopy. Fourier transformation of the time-domain TPI data yields frequency-domain terahertz spectra for each pixel. Thus, in total, TPI analysis generates a four-dimensional data set including vertical and horizontal spatial dimensions, the time (depth) dimension, and the spectral frequency dimension. The terahertz waveforms contain information about the refractive indices of the layered structures, making it possible to image at depth. Although this research proved to be valuable qualitatively, no quantitative estimates of components were provided.

Research conducted by Cogdill et al. [2] demonstrated empirically that both theophylline and lactose showed absorption features in the THz region, while a third (amorphous) component, MCC, demonstrated no real sensitivity. It was suggested that the MCC correlations may have been a consequence of model over-fit; since the w/w concentrations of all tablet constituents in the mixtures summed to one, MCC concentrations were most likely predicted by closure. Using the frequency-domain THz signals, the authors determined a suitable procedure for generating multivariate prediction vectors for quantitative chemical analysis of solid dosage forms. Calibration models were generated by partial least squares, type II (PLS-2) regression of the TPI spectra and by generating a pure-component projection (PCP) basis set using net analyte signal (NAS) processing. Following generation of the calibration vectors, the predictive performance of both methods for predicting theophylline, lactose, and MCC was compared using the validation spectra and by generating chemical images from samples with known composition patterns. The authors note that excellent prediction linearity was observed for the PLS calibration over the range of all constituents for both the calibration and validation datasets. Multi-component prediction images verified the spatial and composition fidelity of the system. The NAS–PCP calibration procedure yielded accurate, linear predictions for theophylline and lactose, while the results for MCC prediction were very poor, due to the relative lack of phonon absorption bands. The results of the study demonstrated the utility of TPI reflection spectroscopy and efficient NAS–PCP for quantitative analysis of crystalline pharmaceutical materials.

This paper expounds upon that of Cogdill et al. [2] by exploring the feasibility of simultaneously calibrating for a four-component tablet of which two components are non-crystalline. In addition to concentration variation, designed density variation at each concentration design point was used to produce density maps.

Powder compaction is a unit operation employed frequently in pharmaceuticals. During compaction, movements take place within the powder bed and interactions occur between the powder and tooling (i.e., the die wall and punch faces). As a result, density variations are induced in the volume of the tablet, which may affect its physical and mechanical properties. Density variations within solid oral dosage forms are important because they may lead to differences in dissolution or mechanical response during post-compaction operations, packaging, storage or use [6].

The objectives of this work were to (1) develop quantitative calibration models for prediction of compact composition for a four-component system which includes two amorphous constituents and (2) investigate the existence of, and physical basis for, any time- or frequency-domain spectral features related to compact density.

2. Experimental

2.1. Four-component tablet production

A model tablet system based on a 29-point quaternary mixture (Table 1) was chosen to provide a realistic chemometric challenge to the method. Anhydrous theophylline powder (Lot No. 92577, Knoll AG, Ludwigshafen, Germany) was chosen as the model compound; lactose 316 Fast Flo NF Monohydrate (Lot No. 8502113061, Hansen Labs, New Berlin, WI), microcrystalline cellulose (MCC, Avicel PH 200, Lot No. M427C, FMC BioPolymer, Mechanicsburgh, PA), and starch (Lot No. 39362, EMD Chemicals, Inc., Gibbstown, NJ) were chosen as compaction excipients. The approximate mean particle size of the theophylline, lactose, MCC and starch (reported by documentation from their respective suppliers), were ∼90, ∼100, ∼180 and ∼17 μm, respectively. All ingredients were used "as is," with no additional characterization or modification of particle size.

Table 1

Tablet #	Theophylline (% w/w)	Lactose (% w/w)	MCC (% w/w)	Starch (% w/w)
1	0.6	0.2	0.2	0
2	0.4	0.4	0.2	0
3	0.2	0.6	0.2	0
4	0.4	0.2	0.4	0
5	0.2	0.4	0.4	0
6	0.2	0.2	0.6	0
7	0.6	0.2	0	0.2
8	0.4	0.4	0	0.2
9	0.2	0.6	0	0.2
10	0.6	0	0.2	0.2
11	0.4	0.2	0.2	0.2
12	0.2	0.4	0.2	0.2
13	0	0.6	0.2	0.2
14	0.4	0	0.4	0.2
15	0.2	0.2	0.4	0.2
16	0	0.4	0.4	0.2
17	0.2	0	0.6	0.2
18	0	0.2	0.6	0.2
19	0.4	0.2	0	0.4
20	0.2	0.4	0	0.4
21	0.4	0	0.2	0.4
22	0.2	0.2	0.2	0.4
23	0	0.4	0.2	0.4
24	0.2	0	0.4	0.4
25	0	0.2	0.4	0.4
26	0.2	0.2	0	0.6
27	0.2	0	0.2	0.6
28	0	0.2	0.2	0.6
29	0.25	0.25	0.25	0.25

Individual components were weighed for each design point (Data Range, Model No. AX504DR, Mettler Toledo, Columbus, OH) on a weight by weight (w/w) basis, and transferred to 25 mL glass scintillation vials. In total, 6000 mg of material was weighed out for each design point, and the nominal weights for all constituents were adjusted to the observed mass data. After the vials were gently agitated for 15 min on a Jar Mill (US Stoneware, East Palestine, OH, USA), a NIR reflectance spectrum was collected directly through the bottom of the glass vial (FOSS NIRSystems 5000, FOSS NIRSystems, Inc., Laurel, MD). Agitation and NIR analysis was continued in 15-min cycles until homogeneity was observed.

Six tablets were produced from the mixture in each vial. The first five tablets produced from the material in each vial were compacted at one of five levels of compaction force (2000, 3500, 5000, 6500, and 8000 lbs) using a Carver Automatic Tablet Press (Model 3887.1SD0A00, Wabash, IN) with flat-faced punches, a 13-mm die, and a dwell time of 10 s. The compaction force for the sixth tablet from each vial was selected from the five levels using a (pseudo) random number generator. The first five tablets from each mixture were combined to create a 145-sample calibration dataset. The sixth tablet from each mixture was set aside for prediction or test data. In total, 174 compacts were produced with a nominal target weight of 800 mg per tablet. In addition, each of the four pure-component materials was directly compacted using the same tablet die and nominal target weight.

Tablet density was calculated from individual tablet dimensions. True density was calculated based on helium pycnometry values for each pure component (Micromeritics Accupyc 1330, Particle & Surface Sciences Pty. Limited, Gosford, New South Wales, Australia); true density values for theophylline, lactose, MCC and starch were 1.491, 1.540, 1.552, and 1.516 g/cm^3, respectively. The true density estimate for each compact was based on the weight fraction of each pure component in the chemical mixture:

$$\rho_{\text{compact}} = (X_1\rho_1) + (X_2\rho_2) + (X_3\rho_3) + (X_4\rho_4) \quad (1)$$

where ρ is true density (g/cm^3) and X is weight fraction (w/w). Data are reported as a ratio of tablet to true density, i.e., relative density.

2.2. Data acquisition, instrumentation, and software

Following compaction, a THz image from one randomly selected side of each tablet was acquired in reflection mode using a TPI Coating Scan (TeraView Limited, Cambridge, UK). A 5-mm diameter spot near the center of each tablet was scanned to reduce any edge effects (e.g., scattering) and to reduce scan time; each scan required approximately 10 min. The spectral range of interest was approximately 8–60 cm^{-1}. Scanning parameters were held constant for all tablets analyzed.

Conversion of the time-domain TPI waveforms to frequency-domain spectra was performed by batch software provided by TeraView. Both refractive index and optical absorption spectra were calculated and subjected to all subsequent data analyses. Chemometric analyses were performed in the MATLAB programming environment (v7.1, The MathWorks, Natick, MA) using the PLS_Toolbox (v3.0, Eigenvector Research, Manson, WA) along with many analysis routines developed in-house (Duquesne University Center for Pharmaceutical Technology-DCPT, Pittsburgh, PA).

2.3. Data analysis

Since an individual spectrum was obtained for each pixel in the terahertz pulsed image, in order to simplify the data analysis process, only the mean spectrum for each tablet was used for calibration and prediction testing of both frequency- and time-domain data. The mean spectrum was obtained by taking the average of the spectra of all pixels in the sample image. It was anticipated that some pretreatment of the frequency-domain spectra would be required to reduce baseline effects related to physical sample interactions [2]. Typical spectroscopic preprocessing operations, such as scatter correction, detrending, and derivatives, as well as combinations of procedures [7], were tested. The preprocessing method chosen for further method development was selected based on reduction of cross-validation error. The root-mean squared error (RMSE) of calibration (RMSEC), cross-validation (RMSECV), and prediction (RMSEP) were calculated for each calibration model.

Empirical modeling of the TPS frequency spectra and concentration data was performed using PLS-2, whereby the regression coefficient vectors for each of the tablet constituents were estimated simultaneously from the same orthogonal basis set [8]. PLS-2 was used for the sake of convenience since there was known correlation among y-variables. The ideal number of PLS latent variables for regression was estimated by minimizing the RMSEC and RMSECV. Between two and six PLS factors were expected to be required for adequate model complexity, based on the number of chemical constituents and physical factors expected to affect the shape of spectra [2]. While high-rank models could be used successfully, calibrations involving significantly more factors than the number of chemical constituents should be approached with caution to avoid over-fitting.

Examination of the raw time-domain data showed a peak shift (not shown); the effect was not associated with the physical or chemical characteristics of the samples, and thus was assumed to be due to some form of instrumental drift. Each time-domain spectrum was corrected for axis shift relative to a single reference spectrum using spline interpolation. Although the effect of the time-domain shift was observed during principal component analysis (PCA) of the frequency-domain data (not shown), no algorithm was available for correction of the frequency-domain spectra during the time of this research.

3. Results and discussion

3.1. Frequency-domain

3.1.1. Analysis of spectra

A comparison of the raw absorbance and refractive index sample spectra and scaled pure components spectra, respectively (Figs. 1 and 2) reaffirmed the higher levels of sensitivity

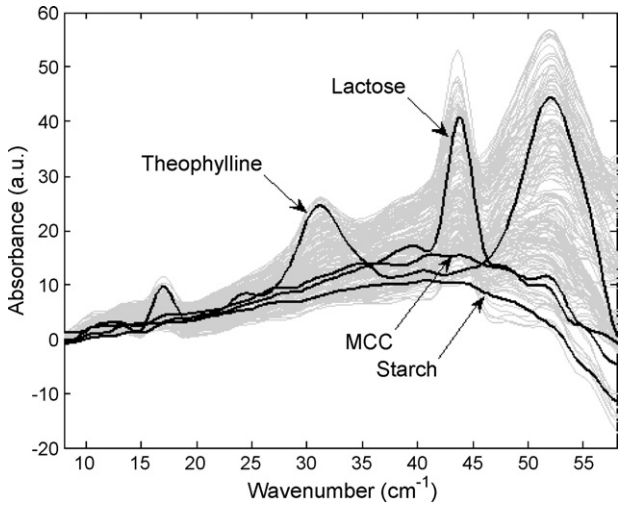

Fig. 1. Overlaid pure-component (black) and raw (gray) tablet optical absorbance spectra.

for crystalline components (i.e., lactose and theophylline) in the terahertz region. Conversely, non-crystalline components, including MCC and starch, appear to be mainly featureless baselines. The lack of terahertz spectral features by non-crystalline or amorphous materials has been connected to the molecules' lack of sufficient long-range order to sustain lattice vibrations [2].

As was described by Cogdill et al. [2], some correspondence can be observed between the absorption and refractive index spectra; qualitatively, the refractive index spectra look similar to a first-derivative profile of the absorption spectra. This correspondence is typical of the anomalous dispersion patterns expected to be observed near absorption bands, and is described by the classical Kramers–Kronig relation [9–11].

The correlation of each constituent to raw optical absorbance or refractive index intensity variables is illustrated in Fig. 3. For optical absorbance, theophylline and lactose were more correlated to the sample spectra at their respective frequencies of THz absorbance, but shared some negatively correlated spectral features with each other which were likely artifacts of the mixture design. Both MCC and starch had, at most, very weak correlations at all frequencies, and were loosely correlated with both crystalline constituents. Lactose had the strongest correlation to the sample refractive index spectra; all other components were very weakly correlated. It is important to keep in mind that, even though there are two amorphous components (expected to have no reliable THz signal), due to the constraints of the mixture design, each constituent has mutual (negative) correlation with the other constituents of −1/3 which is ultimately manifest in the spectral data as false correlation structures.

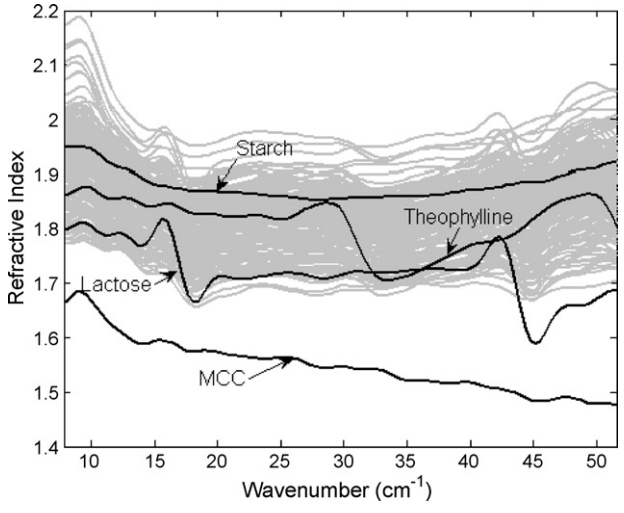

Fig. 2. Overlaid pure-component (black) and raw (gray) refractive index spectra.

The effect of compaction force on sample refractive index spectra was examined by plotting the mean refractive index spectra of all compacts at each compaction level, respectively (Fig. 4). Note that although compaction force increases by the same step size (i.e., 1500 lbs), the peak attenuation plateaus; this may be an indication that features related to tablet density may become saturated at very high compaction forces.

The spectral preprocessing treatment was optimized using cross-validation in conjunction with PLS-2 regression. Ultimately, Savitzky–Golay second derivative (third order polynomial, 9 pt filter) pretreatment [7–12] was selected for the absorption data, and Savitzky–Golay first derivative (second order polynomial, 9 pt filter) pretreatment [7–12] was chosen for the refractive index data. The spectral derivative operations effectively mitigate the baseline shift (not shown). Smoothing derivatives are also useful for amplifying useful features in the spectra.

3.2. Time-domain

3.2.1. Analysis of spectra

Time-domain THz spectra are generated by measuring the intensity of THz reflections over a range of probe beam delays [13]. The features in TPS time-domain spectra correspond to relatively intense reflection events that occur when the incident THz plane wave meets an interface between two materials having different refractive indices. Because the four-component tablet set had no coating layer or discernable intra-tablet interfaces due to inhomogeneities, the only significant features observed in the time-domain spectra of all compacts were caused by the air-tablet interface reflection event, appearing at 0 ps (Fig. 5). The effect of the five levels of compaction force was manifest in the mean attenuated terahertz signal intensities. Note that the same decrease in attenuation of the main peak is observed as in the mean refractive index spectra. No obvious component concentration-related effects were discernible in the raw time-domain spectra.

3.3. PLS calibration

3.3.1. Chemical composition

The optimization and performance statistics for the PLS four-component calibrations are summarized in Table 2. Five and four PLS latent variables (i.e., model factors) were used to model both the optical absorption and refractive index spectra for the four-component calibrations, respectively. The optimal

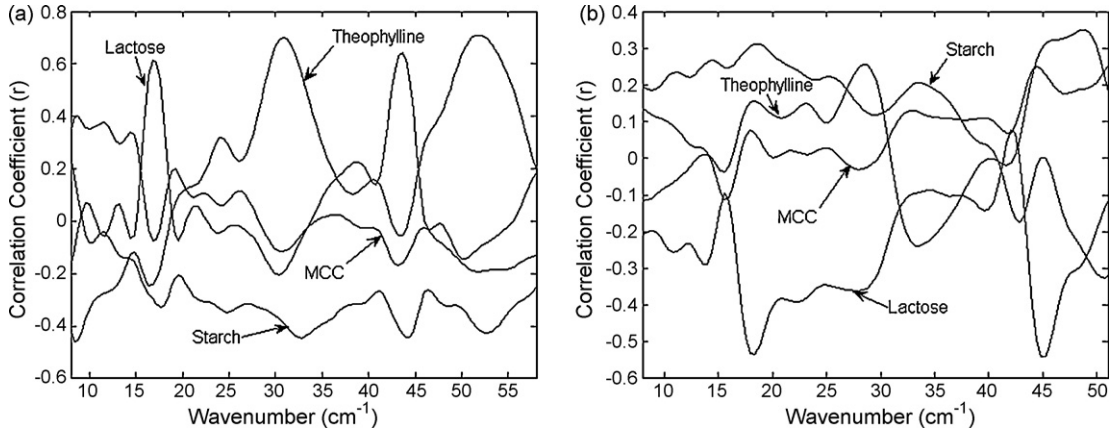

Fig. 3. Correlation of each pure-component to the raw tablet optical absorbance (a) and refractive index (b) spectra.

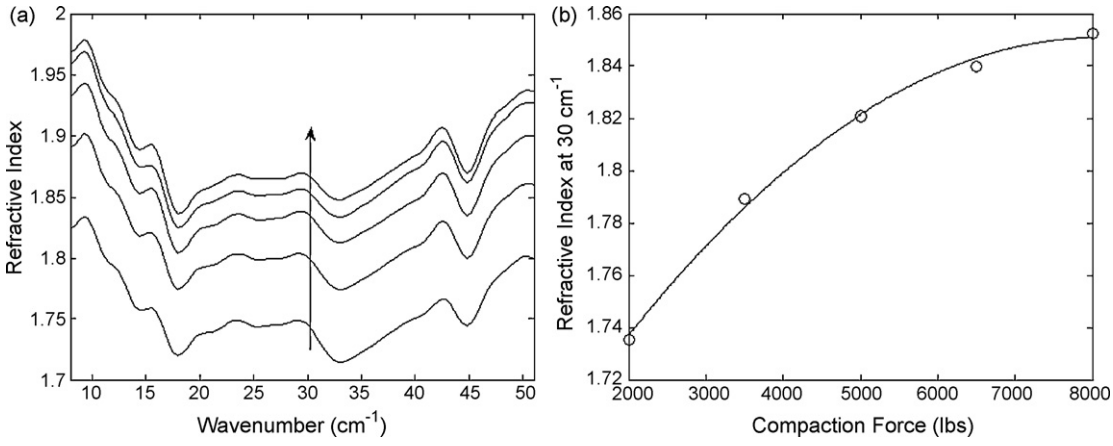

Fig. 4. Effect of compaction force (2000, 3500, 5000, 6500 and 8000 lbs) on the mean refractive index spectra of all compacts. The arrow indicates the direction of increasing force.

PLS rank of each calibration was chosen based on interpretation of the RMSECV scree plot (illustrating the trend of RMSECV as related to the model rank); the PLS rank after which RMSECV failed to improve appreciably was selected. Both calibration and cross-validation performance was very good for both crystalline constituents; predictions for MCC and starch were considerably worse.

It was expected that a model with fewer latent variables and comparable performance could be obtained by a pseudo-three-component model, where the concentration columns of both amorphous components were added to represent a single class of component. Three and two latent variables were used to model absorbance and refractive index in these reduced calibrations, respectively (Table 3). Also note that no derivatives were required to model optical absorbance as a three-component system. Although the predictability of the crystalline materials' concentrations remained approximately the same for both pseudo-three-component models, the mean RMSEC and

Table 2

Data type	Optical absorbance (full model)				Refractive index (full model)			
Method	PLS				PLS			
Preprocessing	Second derivative (9, 3, 2)				First derivative (9, 2, 1)			
Latent variables	5				4			
RMSEC (w/w)	0.075				0.070			
RMSECV (w/w)	0.080				0.073			
RMSEP (w/w)	0.074				0.070			
Constituent	Theophylline	Lactose	MCC	Starch	Theophylline	Lactose	MCC	Starch
R^2_{cat}	0.927	0.912	0.638	0.752	0.929	0.900	0.748	0.780
R^2_{cval}	0.918	0.898	0.590	0.722	0.918	0.926	0.702	0.806
R^2_{val}	0.917	0.916	0.631	0.802	0.924	0.891	0.727	0.758

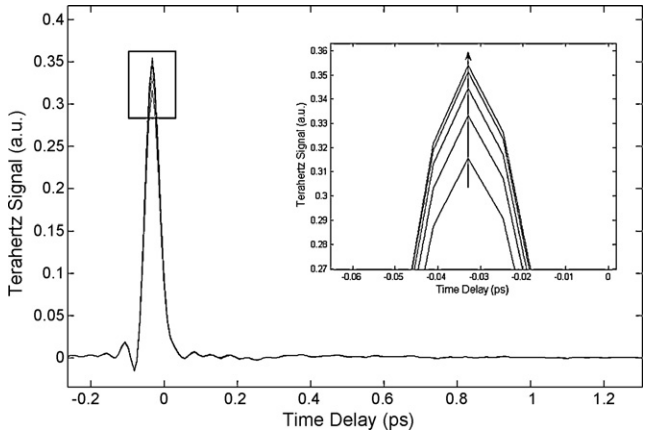

Fig. 5. Mean time-domain spectra at each compaction force (2000, 3500, 5000, 6500, and 8000 lbs, respectively). Inset: Effect of compaction force, enhanced view. The arrow indicates the direction of increasing force.

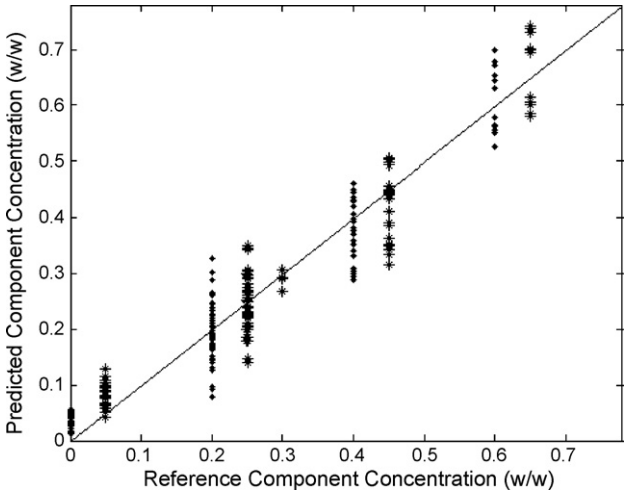

Fig. 7. Measured vs. predicted absorbance validation component concentrations for theophylline and lactose using three- (circle) and four-component (triangle) validation data. The two data sets are offset for clarity.

RMSECV, as well as RMSEP for these models, respectively, were reduced when compared to four-component models. While the optical absorbance model had little sensitivity with respect to the amorphous content, the refractive index model had high sensitivity.

The absorbance and refractive index PLS regression vectors (Fig. 6) may be related to the sensitivity of the models to each pure component, respectively. The four-component calibration regression vectors for both theophylline and lactose were highly correlated to their pure component spectra, indicating that there was adequate sensitivity for these constituents. However, it appeared that both MCC and starch were mostly correlated to the loss of either crystalline component, indicating that clo-

Table 3

Data type	Optical absorbance (three-component model)			Refractive index (three-component model)		
Method	PLS			PLS		
Preprocessing	N/A (mean-centered only)			First derivative (9, 2, 1)		
Latent variables	3			2		
RMSEC (w/w)	0.056			0.060		
RMSECV (w/w)	0.060			0.062		
RMSEP (w/w)	0.057			0.054		
Constituent	Theophylline	Lactose	Other	Theophylline	Lactose	Other
R^2_{cal}	0.935	0.906	0.891	0.918	0.898	0.884
R^2_{cval}	0.927	0.899	0.879	0.915	0.895	0.878
R^2_{val}	0.927	0.915	0.887	0.910	0.922	0.922

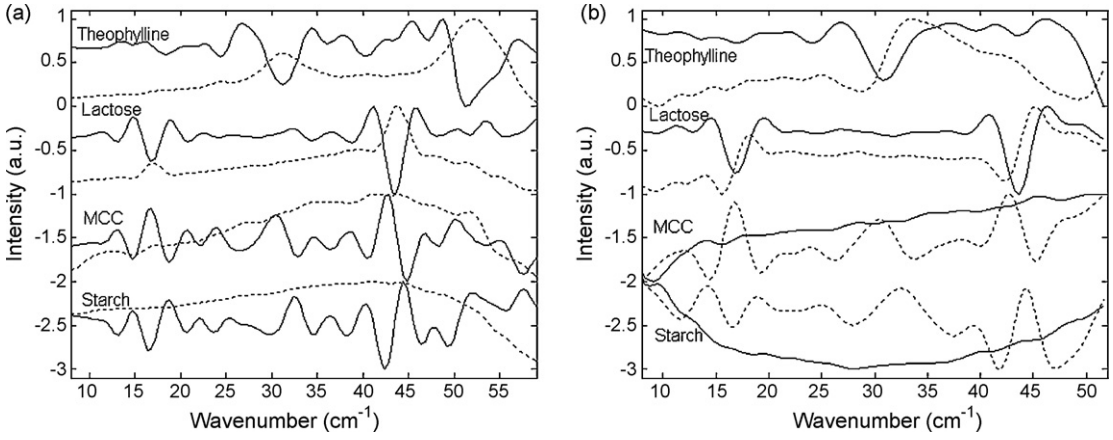

Fig. 6. PLS regression vectors for 4-component absorbance (a) and refractive index (b) spectra overlaid with pure-component spectra. Solid and dashed lines refer to theophylline, lactose, MCC and starch regression vectors and pure-component spectra, respectively.

Table 4

Data type	Refractive index	Time-domain
Method	PLS	
Preprocessing	N/A (mean-centered)	
Latent variables	5	4
RMSEC	0.012	0.011
RMSECV	0.013	0.012
RMSEP	0.011	0.012
R^2_{cal}	0.937	0.948
R^2_{cval}	0.927	0.941
R^2_{val}	0.952	0.949

sure may have been a factor in determining the concentration of these constituents. This lack of sensitivity substantiates the decline in predictive performance at higher concentrations of these constituents (not shown).

Theophylline and lactose concentration predictions (combined) are illustrated in Fig. 7, where three- and four-component prediction sets (i.e., test sets) are offset for comparison purposes. This plot reiterates the fact that a pseudo-3-component model, which uses fewer latent variables and no preprocessing, is as satisfactory a predictor of component concentration for crystalline materials as a higher-factor four-component model.

3.3.2. Tablet density

Both univariate and multivariate calibration methods (Table 4) were used to model the spectral effect of compact density variation (Fig. 8). The correlation between reference compact density and the time-domain traces was greatest at 0 ps delay time, i.e., the air-tablet interface. Therefore, based on the assumption that tablet density is mostly a surface phenomenon, using only the variable corresponding to 0 ps time-delay, a correlation coefficient (R^2) of 0.759 was calculated. However, multivariate refractive index and time-domain calibrations using PLS-regression methods greatly increased the R^2 statistic to 0.937 and 0.948, respectively. The PLS algorithm identifies the orthogonal linear basis having maximum covariance with the reference (target) variable [8]. Hence, as the inclusion of time-domain signals relating to depths below the compact surface significantly increased the prediction performance of the calibration, it might be speculated that the time-domain spectra are sensitive to density variations within the compact volume.

Since the time-domain spectral features are primarily attributed to refractive interfaces at depth, however, it is difficult to conclude that most of the tablets had regular intervals of density variation along their cross-section. Also, it is important to bear in mind that, whether considering the time- or frequency-domain spectra, the same information content is analyzed; the Fourier transformation operation simply changes the basis. Thus, with regard to density, both the time- and frequency-domain correlations might ultimately be attributable to spectral effects caused by multiple-pass interference at the air-tablet interface, rather than sub-surface features. For these reasons,

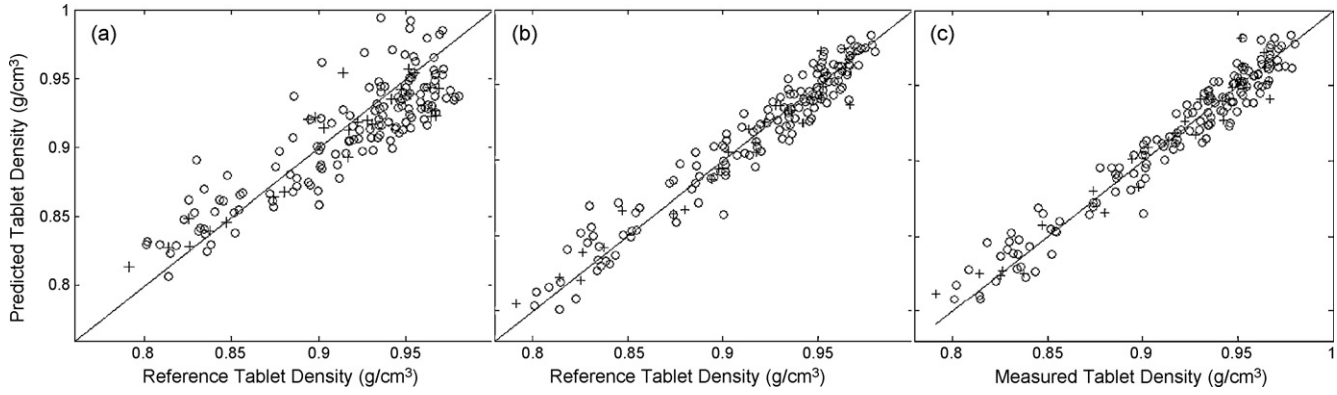

Fig. 8. Calibration (◯) and validation (+) PLS predictions for compact density using an univariate time-domain calibration (a) and multivariate refractive index calibration and time-domain calibrations (b,c), respectively. The solid line in each plot represents the ideal (unity slope) prediction line.

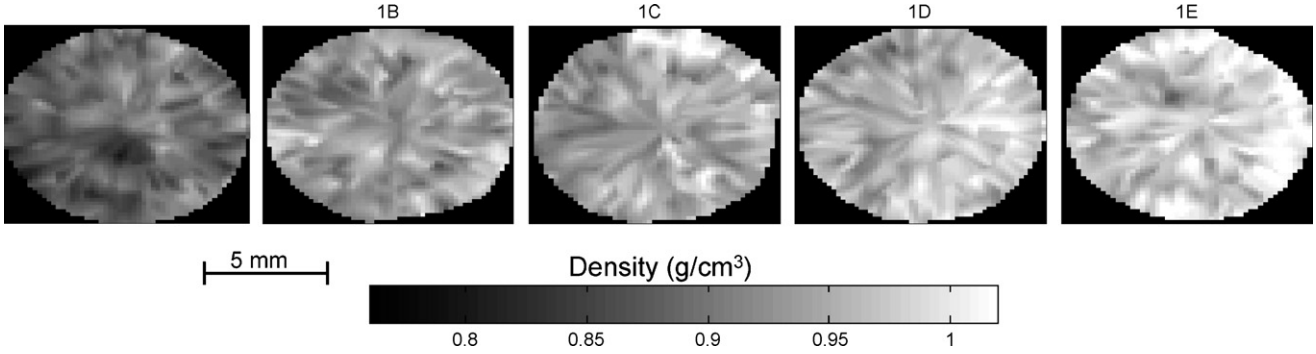

Fig. 9. Surface density maps. One example image is shown for each compaction level of one concentration design point. The false-color bar illustrates density predictions at each pixel.

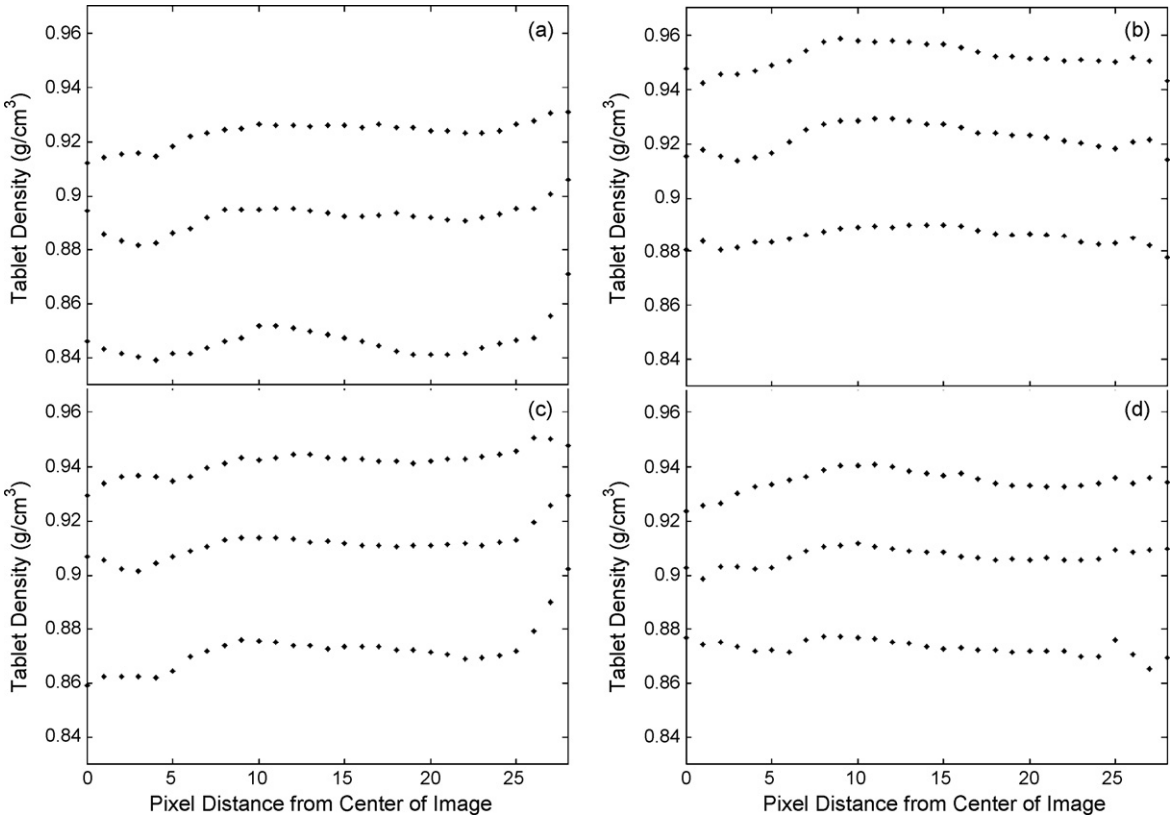

Fig. 10. Plots of 25th, 50th and 75th percentiles (bottom to top, respectively) of density predictions at increasing pixel distances from center of compact images. Compacts were divided into subsets in which either theophylline (a), lactose (b), MCC (c), or starch (d) were absent from the concentration design.

the true nature of the full-spectrum time-domain correlation to tablet density variation cannot be explained using only these data, and will require additional investigations.

Calibration and prediction set statistics for each calibration model are illustrated in Table 4. Although univariate model predictions were reasonable (R^2 values for calibration and prediction were 0.871 and 0.924, respectively), many tablet densities were grossly overestimated (Fig. 8a). Predictions based on the multivariate refractive index calibration were enhanced over the univariate prediction (R^2 values for calibration and prediction were 0.937 and 0.952, respectively), but were inadequately described at low reference tablet density values (Fig. 8b). The predictive ability of the multivariate time-domain calibration was much improved over the univariate calibration and slightly enhanced over the frequency-domain calibration (R^2 for calibration and prediction were 0.948 and 0.949, respectively).

Tablet density on a pixel-to-pixel basis was investigated by applying the refractive index calibration to each pixel of a tablet image (collected via the TPI Coating Scan). A false-color image was created which illustrates compact density predictions across the surface of each tablet. A series of tablets from one concentration design point, spanning each compaction level, is presented in Fig. 9. Radial striations of higher tablet density were observed in all images, which may be an artifact of the compaction mechanism or an artifact of the instrument, itself.

The density of compacts at increasing pixel distances from the center of each image as a function of the chemical components present was investigated using percentile plots. In Fig. 10, a percentile plot (including the 25, 50, and 75th percentiles) was created using the mean refractive index spectra of each "class" of compacts; a class was defined as a group of compacts in which the concentration design excluded one constituent (i.e., 0% w/w). The mean of the predicted tablet densities across all pixels for tablets lacking theophylline, lactose, MCC or starch are 0.884, 0.918, 0.907, and 0.902 g/cm^3, respectively. These values are very comparable to the average calculated tablet densities for each group. True edge effects due to compaction mechanisms (caused by tooling or otherwise) were not observed since the compact radius was limited during initial data collection; however, it was thought a general trend may manifest itself. Here, an increase in tablet density near the edge of the image is observed in most cases.

The plots in Fig. 10 suggest that the presence of lactose tends to suppress overall compact density more than any other component, as the mean density for tablets not including lactose tend to have higher tablet density, indicating that lactose is the least compactable component and has the most intense effect on overall tablet compactability or deformability. At any compaction force, those compacts not containing theophylline tend to have a reduced density. It is speculated that this effect was related to the small particle size of theophylline relative to the other raw materials.

These results can be related to the importance of homogenous blending on physical tablet properties, which consequently affect therapeutic qualities of a solid dosage form. Aside from inappropriate drug dosing, compacting an inhomogeneous powder blend with a disproportionate amount of theophylline could lead to a distinctly different density profile, and hence, dissolution profile.

4. Concluding remarks

The results of this study have illustrated a procedure by which TPS can be used in conjunction with multiple chemometric tools for quantitative chemical and density mapping of pharmaceutical materials. It is noted that while the concentration of crystalline materials can be predicted with confidence, by combining all amorphous species into a single group, the need for more complex preprocessing methods and the number of latent variables required for modeling are both decreased. Based on this research, there is an apparent advantage to using optical absorption for chemical method development, and refractive index or time-domain data for density method development.

Future work in this area will include looking at density features and chemical signals at depth within a tablet to generate a three-dimensional image which can be correlated to both physical properties and product performance attributes.

Acknowledgements

The authors would like to kindly Jonathan Gortat at Purdue University for graciously performing the helium pycnometry analysis.

References

[1] D. Grischkowsky, S. Keiding, M. van Exter, C. Fattinger, J. Opt. Soc. Am. B 7 (1990) 2006–2015.
[2] R.P. Cogdill, C.A. Anderson, J. Near Infrared Spectrosc. 13 (2005) 119–132.
[3] Y.C. Shen, P.F. Taday, D.A. Newnham, M. Pepper, Semicond. Sci. Technol. 20 (2005) 254–257.
[4] Y. Watanabe, K. Kawase, T. Ikari, H. Ito, Y. Ishikawa, H. Minamide, Opt. Commun. 234 (2004) 125–129.
[5] Y. Watanabe, K. Kawase, T. Ikari, H. Ito, Y. Ishikawa, H. Minamide, Appl. Phys. Lett. 83 (2003) 800–802.
[6] I.C. Sinka, S.F. Burch, J.H. Tweed, J.C. Cunningham, Int. J. Pharm. 271 (2004) 215–224.
[7] R.P. Cogdill, C.A. Anderson, M. Delgado-Lopez, R. Chisholm, R. Bolton, T. Herkert, A.M. Afnan, J.K. Drennen, AAPS PharmSciTech 6 (2005).
[8] S. De Jong, Chemom. Intell. Lab. Syst. 18 (1993) 251–263.
[9] G. Mouret, S. Matton, R. Bocquet, D. Bigourd, F. Hindle, A. Cuisset, J.F. Lampin, D. Lippens, Appl. Phys. Lett. 88 (2006), 181105/1-181105/3.
[10] B. Yu, F. Zeng, Y. Yang, Q. Xing, A. Chechin, X. Xin, I. Zeylikovich, R.R. Alfano, Biophys. J. 86 (2004) 1649–1654.
[11] R. Parthasarathy, T. Globus, T. Khromova, N. Swami, D. Woolard, Appl. Phys. Lett. 87 (2005), 113901/1-113901/3.
[12] A. Savitzky, M.J.E. Golay, Anal. Chem. 36 (1964) 1627–1639.
[13] A.J. Fitzgerald, B.E. Cole, P.F. Taday, J. Pharm. Sci. 94 (2004) 177–183.